Supplemental Material for "Orbital Floquet engineering of Exchange Interactions in Magnetic Materials"

Swati Chaudhary, David Hsieh, and Gil Refael
Institute of Quantum Information and Matter, Department of Physics, California Institute of Technology, Pasadena, California 91125, USA

I. REVIEW : TOY MODEL FOR AFM COUPLING RENORMALIZATION DUE TO PHOTO-MODIFIED DIRECT HOPPING

We briefly review the effect of a periodic drive on the exchange interactions using the periodically driven Fermi Hubbard model (FHM) in Mott regime at half-filling. In the presence of a time dependent electric field, the full Hamiltonian of the Fermi-Hubbard model is given by:

$$H = -t \sum_{<i,j>} c^{\dagger}_{i\sigma} c_{j\sigma} + \text{h.c} + U \sum_{i} n_{i\uparrow} n_{i\downarrow} + \mathbf{E}\cdot \sum_{\mathbf{i},\sigma} n_{i\sigma} \mathbf{r_j} \cos(\omega \mathbf{t}). \tag{1}$$

After Peierls substitution, it becomes:

$$H' = -t \sum_{<i,j>} e^{i\left[\frac{\mathbf{E}\cdot(\mathbf{r_j}-\mathbf{r_i})}{\omega}\sin(\omega t)\right]} c^{\dagger}_{i\sigma} c_{j\sigma} + \text{h.c} + H_U = H'_t + H_U. \tag{2}$$

In the limit $U \gg t$, and for a non-resonant drive, the exchange coupling is given by:

$$J'_i = J_i U \sum_{n=-\infty}^{\infty} \frac{1}{U + n\omega} \mathcal{J}_n(\zeta_i)^2, \tag{3}$$

where, $J_i = \frac{4t^2}{U}$ is the magnetic coupling strength for the undriven case, $\mathcal{J}_n$ denotes n^{th} order Bessel function, and drive parameter

$$\zeta_i = \frac{\mathbf{E}\cdot(\mathbf{r}_j - \mathbf{r}_i)}{\omega}. \tag{4}$$

In the presence of this periodic drive, the spin exchange interactions are affected mainly due to two factors: (a) change in the hopping parameter due to photon-assisted tunneling (b) virtual excitations between different Floquet sectors as shown in Fig. 3 of Ref. [1]. As a result, the effective spin exchange interactions can be controlled by changing the frequency, polarization and intensity of the laser. Previous works [1–6] have studied the periodically driven FHM extensively for both resonant and off-resonant cases. The above expression in Eq. (3) is valid only for a non-resonant drive where doublon sectors are well separated in energy from the single occupation sector. Resonant drive can be handled using a somewhat similar machinery of Floquet formalism as shown in Ref. [4]. For a near resonant drive, real doublon-holon pairs can significantly affect the exchange interactions and its effects are discussed in great details in Ref. [7].

II. AFM EXCHANGE VIA TWO ORBITALS OF THE SAME LIGAND ION IN THE PRESENCE OF A PERIODIC DRIVE

When the hopping between two metal sites is allowed via two orbitals of the ligand ion, spin exchange energy for undriven case is given by :

$$J_{ex} = 4 \sum_{\alpha=A,B} t_{\alpha}^4 \left(\frac{1}{\Delta_{\alpha i}^2 U} + \frac{1}{\Delta_{\alpha i}^3}\right) + \frac{8 t_A^2 t_B^2}{\Delta_{Ai}\Delta_{Bi} U} + 4 t_A^2 t_B^2 \left(\frac{1}{\Delta_{Ai}\Delta_{Bi}\Delta_{ABi}} + \frac{1}{\Delta_{Ai}^2 \Delta_{ABi}} + \frac{1}{\Delta_{Bi}^2 \Delta_{ABi}}\right), \tag{5}$$

where, $\Delta_{\alpha i} = U - E_{\alpha}$ is the charge transfer gap, and $\Delta_{ABi} = (\Delta_{Ai} + \Delta_{Bi})/2$. This expression was obtained by applying fourth order perturbation theory to the following hamiltonian:

$$H_1 = H_0 + H_t = \sum_{\alpha=A,B} \sum_{\sigma} E_{\alpha} n_{\alpha\sigma} + U \sum_{i=1,2} n_{i\uparrow} n_{i\downarrow} - \sum_{i=1,2} \sum_{\alpha} t_{\alpha} c^{\dagger}_{\alpha\sigma} c_{i\sigma} + \text{h.c} \tag{6}$$

where $\alpha = A, B$ are two orbitals of the ligand ion involved in the process of superexchange between the spins at two metal sites denoted by $i = 1, 2$ above, and the hopping parameter $t_{A/B} \ll U, |E_{\alpha}|$.

In this case, spin exchange energy is decided by the virtual excitations which lead to spin exchange between two sites, and thus depends on the number of orbitals available for the exchange process and the energy of these orbitals. There are multiple pathways available for these spin exchange processes. Two such exchange processes are shown in Fig. 1, where we have shown the virtual excitations giving rise to the magnetic interactions between two metal ions. These virtual excitations involve the charge transfer from ligand orbitals to the magnetic ion. Their contribution to magnetic coupling depends on the energy difference between obitals and the on-site columbic repulsions. In the presence of a drive discussed in Sec. IV, these orbitals of the ligand ion are modified according to the drive amplitude and frequency. Now, we proceed in the same way as the undriven case, but the orbitals A and B are replaced by the hybrid orbitals:

$$\begin{aligned} |P, n\rangle &= \cos\frac{\theta}{2} |A, n\rangle + \sin\frac{\theta}{2} |B, n+1\rangle, \\ |M, n\rangle &= \sin\frac{\theta}{2} |A, n\rangle - \cos\frac{\theta}{2} |B, n+1\rangle, \end{aligned} \tag{7}$$

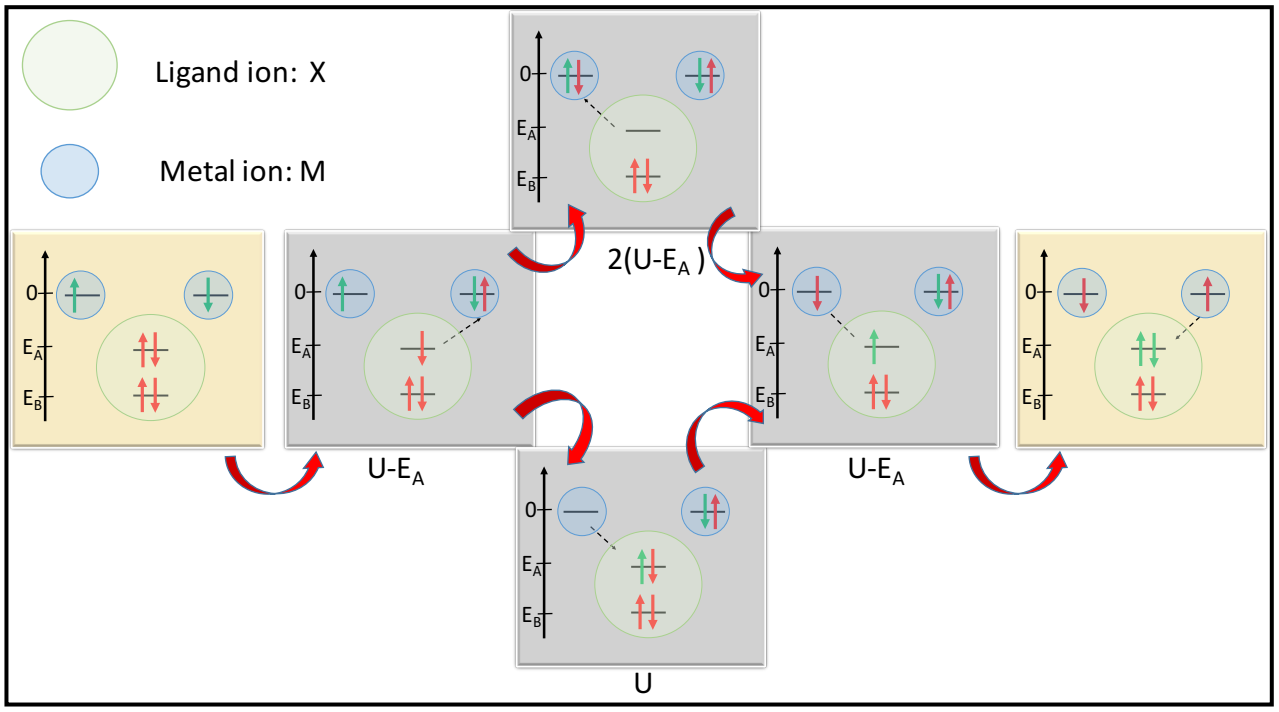

FIG. 1: Two possible spin exchange processes when the hopping between two metal sites is mediated via ligand orbitals. Gray panels show virtual intermediate states with their energies relative to the ground state with one spin on each metal site. Here, the ligand ion has two orbitals, and as a result there are many other channels available for spin exchange if the hopping between orbital B and metal sites is allowed.

where n denotes the Floquet index, $\cos\theta = \frac{\delta}{\sqrt{\delta^2+4\Omega^2}}$, $\sin\theta = -\frac{2\Omega}{\sqrt{\delta^2+4\Omega^2}}$, and $\delta = \omega - \omega_0$ is the detuning. If the parameter $eEa/\omega \ll 1$ (which is the case here, as $\omega \approx 10eV$ and $eEa \approx 1eV$), then the hopping is allowed between orbitals within the same photon sector only in the Floquet picture. Using this fact, we can calculate the hopping elements between metal sites, and the new orbitals can be expressed as:

$$t_P = \langle A,0|P,0\rangle\, t_A + \langle B,0|P,0\rangle\, t_B = \cos\frac{\theta}{2} t_A, \tag{8}$$

$$t_M = \langle A,0|M,0\rangle\, t_A + \langle B,0|M,0\rangle\, t_B = \sin\frac{\theta}{2} t_A. \tag{9}$$

Now, if $t_B \neq 0$, the hopping element between $|P/M,-1\rangle$ and metal sites can still be non-zero as:

$$\begin{aligned} |P,-1\rangle &= \cos\frac{\theta}{2}\,|A,-1\rangle + \sin\frac{\theta}{2}\,|B,0\rangle\,, \\ |M,-1\rangle &= \sin\frac{\theta}{2}\,|A,-1\rangle - \cos\frac{\theta}{2}\,|B,0\rangle\,, \end{aligned} \tag{10}$$

with

$$t_{P1} = \langle A,0|P,-1\rangle\, t_A + \langle B,0|P,-1\rangle\, t_B = \sin\frac{\theta}{2} t_B, \tag{11}$$

and

$$t_{M1} = \langle A,0|M,-1\rangle\, t_A + \langle B,0|M,-1\rangle\, t_B = -\cos\frac{\theta}{2} t_B. \tag{12}$$

As a result of the drive

$$H(t) = \Omega e^{-i\omega t} c^\dagger_{A\sigma} c_{B\sigma} + \Omega^* e^{i\omega t} c^\dagger_{B\sigma} c_{A\sigma}, \tag{13}$$

the magnetic coupling strength now has contributions from different exchange mechanisms which include virtual excitations via four states, i.e $|P\rangle$, $|M\rangle$, $|P,-1\rangle$, $|M,-1\rangle$ given by:

$$J_{ex} = E_0 + E_1 + E_2 \tag{14}$$

where

$$E_0 = \sum_{\alpha=P,M,P1,M1} \frac{4t_\alpha^4}{\Delta_\alpha^2}\left(\frac{1}{U} + \frac{1}{\Delta_\alpha}\right) \tag{15}$$

$$\begin{aligned} E_1 = \frac{1}{2}\sum_\beta \sum_{\alpha,\alpha\neq\beta} &\frac{8t_\alpha^2 t_\beta^2}{(\Delta_\alpha+\Delta_\beta)\Delta_\alpha\Delta_\beta} + \frac{4t_\alpha^2 t_\beta^2}{(\Delta_\alpha+\Delta_\beta)\Delta_\alpha^2} \\ &+ \frac{4t_\alpha^2 t_\beta^2}{(\Delta_\alpha+\Delta_\beta)\Delta_\beta^2} + \frac{8t_\alpha^2 t_\beta^2}{U\Delta_\alpha\Delta_\beta}, \end{aligned} \tag{16}$$

and

$$\begin{aligned} E_2 = &\frac{8t_P t_{P1} t_M t_{M1}}{\Delta_{P1} U_{m1} \Delta_{M1}} + \frac{8t_P t_{P1} t_{M1} t_M}{\Delta_P U_1 \Delta_M} + \frac{4t_P t_{P1}^2 t_P}{\Delta_P U_1 \Delta_P} \\ &+ \frac{4t_M t_{M1}^2 t_M}{\Delta_M U_1 \Delta_M} + \frac{4t_P^2 t_{P1}^2}{\Delta_{P1} U_{m1} \Delta_{P1}} + \frac{4t_M^2 t_{M1}^2}{\Delta_{M1} U_{m1} \Delta_{M1}}, \end{aligned} \tag{17}$$

where, $\Delta_\alpha = U - E_\alpha$, $U_1 = U + \omega$, $U_{m1} = U - \omega$ with

$$E_{P/M} = E_A + \frac{\delta}{2} \mp \sqrt{\left(\frac{\delta}{2}\right)^2 + \Omega^2}, \tag{18}$$

and

$$E_{P1/M1} = E_{P/M} - \omega \tag{19}$$

is the energy of Floquet states $|P/M, -1\rangle$. If we consider a very simple situation where $\Delta_A \gg U, \Delta_A >> \Delta_B, \delta = 0$, then in the undriven case the magnetic coupling strength is $J_{ex} = 4\frac{t_A^4}{\Delta_A^2 U}$, and for the driven case it is given by:

$$J_{ex} = \frac{4}{U}\left(\frac{t_P^2}{\Delta_A + \Omega} + \frac{t_M^2}{\Delta_A - \Omega}\right) \tag{20}$$

where now $t_P = t_M = t_A/\sqrt{2}$, and thus the change depends mainly on the ratio Ω/Δ_A. In order to understand the effect of detuning, let us consider a somewhat simple situation $t_b = 0$ and small drive strength. Now, the virtual excitation involves two states with energy $E_P \approx E_A + \delta + \frac{\Omega^2}{\delta}$ and $E_M \approx E_A - \frac{\Omega^2}{\delta}$ and the corresponding hopping amplitudes are $t_P = \frac{\Omega}{\delta}$ and $t_M = 1 - \frac{\Omega^2}{2\delta^2}$ respectively. In this case, large detuning δ brings the level E_P much closer to d orbitals in energy, and hence the virtual excitation energy is reduced as δ increases. Also, the detuning values are quite close to charge-transfer gap Δ, and thus the change in the magnetic coupling increases with large detuning. This picture was further verified by the numerical calculations as shown in Fig. 2 where we plot the change in magnetic coupling strength as a function of Ω/Δ for different values of detuning δ.

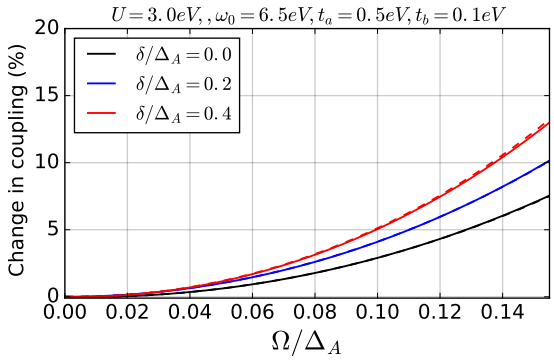

FIG. 2: Change in magnetic coupling as a function of Ω/Δ for ligand orbital scheme for different values of detuning δ. These changes occur mainly due to change in the virtual excitation energy which decreases as detuning increases. This decrease in virtual excitation energy enhances the exchange interactions and thus the change is larger for large detuning.

III. CHANGES IN AFM COUPLING DUE TO ORBITAL HYBRIDIZATION ON EACH METAL SITE

In the undriven model, the spin interactions arise due to virtual excitations between singly and doubly occupied sectors. For large U, the low energy subspace is described by an effective spin hamiltonian. In the presence of a periodic drive which couples two orbital on each metal site, all the states in this subspaces undergo some changes. These changes are best studied using the Floquet formalism, where many singly occupied states now hybridize and the new levels are given by the eigenstates of Floquet hamiltonian. Usually the hopping amplitudes are much smaller in comparison to other energy scales in the problem, and thus we treat the hopping part of the hamiltonian as a perturbation to Floquet hamiltonian obtained from $H_k + H_0 + H(t)$. The schematic of the changes in the energy levels of this hamiltonian is shown in Fig. 3 as a function of the drive amplitude for some of the eigenstates relevant for the exchange interactions.

For the undriven case, there is only one energy eigenstate available for virtual excitations to the doubly occupied sector as denoted by the dashed arrow in Fig. 3. This virtual process lifts the degeneracy between singlet and triplet sectors resulting in a magnetic coupling strength $\frac{4t_A^2}{U}$. For the driven case, the low energy subspace is replaced by the eigenstates of the Rabi hamiltonian:

$$H_{R_P} = \begin{bmatrix} 0 & \Omega\sqrt{2} & 0 \\ \Omega\sqrt{2} & -\delta & \Omega\sqrt{2} \\ 0 & \Omega\sqrt{2} & -2\delta \end{bmatrix} \tag{21}$$

with basis vectors given by $|P_{AA}^{s/t}, 0\rangle, |P_{AB}^{s/t}, -1\rangle, |P_{BB}^{s/t}, -2\rangle$ where P denotes the singly occupied sector with subscripts denoting the orbitals on each site, s/t refers to the singlet and triplet sectors, and the integers denote the photon number. For the singly occupied sector, the effects of drive are independent of the spin configuration. This drive also mixes the doubly occupied subspace for the singlet sector in a similar manner but in this case the energy levels are given by eigenstates of the following hamiltonian:

$$H_{R_{D_s}} = \begin{bmatrix} U & \Omega\sqrt{2} & 0 \\ \Omega\sqrt{2} & U_1 + J - \delta & \Omega\sqrt{2} \\ 0 & \Omega\sqrt{2} & U - 2\delta \end{bmatrix} \tag{22}$$

which give rise to a different energy shift for the two sectors if $U_1 + J \neq U$. On the other hand, for the triplet sector, the doubly occupied subspace consists of is only one state at energy $U_1 - J - \delta$. In addition to the changes in the energy levels this drive also changes the eigenstates, and thus the hopping parameters are changed accordingly. The hopping processes in the presence of a periodic drive are shown by solid arrows in Fig. 3.

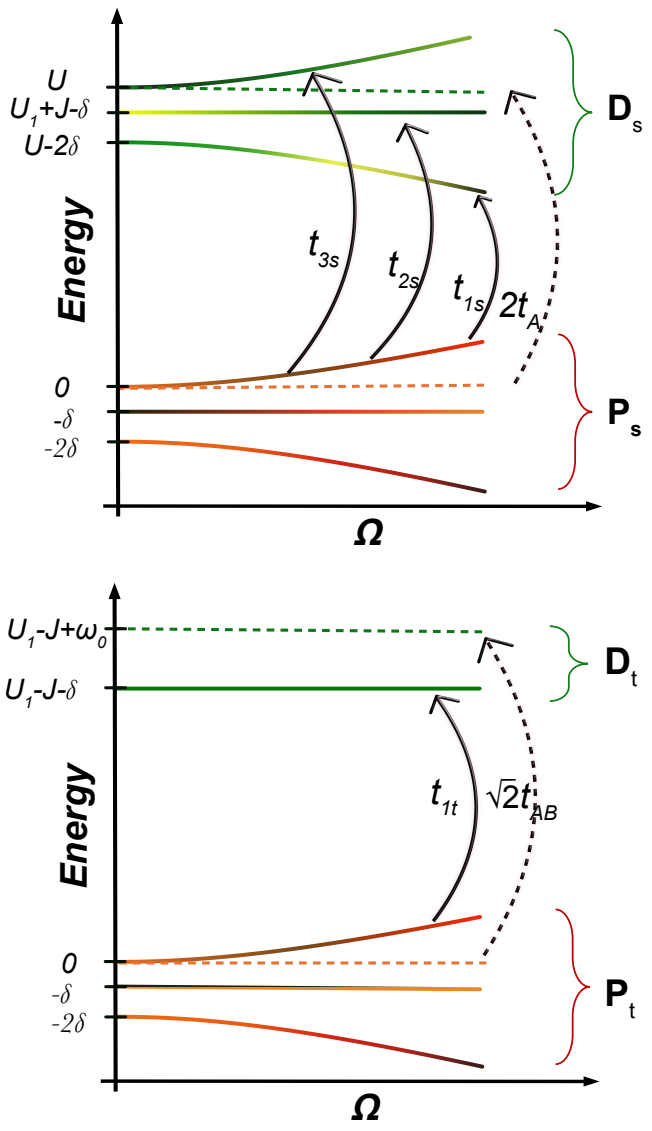

FIG. 3: This diagram shows the effect of the periodic drive on the energy levels of a two metal site and two orbital model discussed in Eq. 21 and Eq. 22. The lower levels shown in shades of red represent the states connected to the low energy subspace of the undriven model, and the lines in green show the states available for virtual excitations which belong to the doubly occupied sector. These excitations are shown by solid arrows for the driven model, and by the dashed arrow for the undriven case. For clarity, we show the excitations for the singlet (top) and triplet (bottom) sectors in different diagrams. Here the subspace P and D refers to the singly and doubly occupied states respectively, and the subscript t/s denotes the singlet or triplet nature.

In terms of these hopping amplitudes, the new magnetic coupling strength is given by:

$$E_s - E_t = \sum_{i=1}^{3} \frac{t_{is}^2}{E_{d_s}^i - E_{p_s}^1} - \sum_i \frac{t_{it}^2}{E_{d_t}^i - E_{p_t}^1} \tag{23}$$

where $E_{d_{s/t}}^i$ is the energy corresponding to the eigenstate $|D_{s/t}\rangle$ of hamiltonian $H_{R_{D_{s/t}}}$ in Eq. 22, and

$$t_{is/t} = \langle P_{s/t}^1 | H_t | D_{s/t}^i \rangle, \tag{24}$$

where $|P_{s/t}^1\rangle$ is the eigenstate corresponding to the eigenvalue $\delta\left(1 - \sqrt{1 + 2\left(\frac{\Omega}{\delta}\right)^2}\right)$ of the hamiltonian H_{R_P} for the singly occupied sector, and H_t is the hopping part given by:

$$H_t = -\sum_{\sigma,\alpha=A,B} t_\alpha c_{1\alpha\sigma}^\dagger c_{2\alpha\sigma} - t_{AB} \sum_{\sigma,i\neq j} c_{1A\sigma}^\dagger c_{2B\sigma} + \text{h.c}, \tag{25}$$

One of the most important contribution to exchange coupling comes from the virtual excitation to the eigenstate with energy $U_1 \pm J - \delta$. If we consider a simple scenario with $t_a = t_b$ and $t_{ab} = 0$, then the virtual hopping to $U_1 - J - \delta$ in the triplet sector, $t_{1t} = 0$, and for $U_1 + J - \delta$ in the singlet sector is given by $t_{2s} \approx \frac{\Omega}{\delta} t_b$ which decreases as the detuning δ increases. Although the detuning also affects the energy of the virtual excitation associated with $U_1 + J - \delta$, the change in exchange energy is dictated by $\frac{\Omega}{\delta}$ mainly as the change in δ is negligible in comparison to $U_1 + J = U - J$. This explains why the observed change decreases with increased detuning. It is also in good agreement with the numerical results shown in Fig. 4 where we plotted the change in magnetic coupling as a function of Ω/δ. Furthermore, the presence of two orbitals can allow virtual processes even for the triplet sector which changes the energy of the FM state when $t_a \neq t_b$ or $t_{ab} \neq 0$.

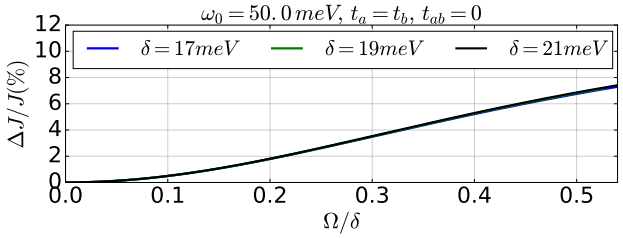

FIG. 4: Change in magnetic coupling as a function of Ω/δ for metal orbital scheme. For the special case where $t_{ab} = 0$, these changes depend on the hybridization between A and B orbitals which is a function of Ω/δ and thus for a given drive strength Ω, the observed change is larger for small detuning.

IV. APPROXIMATE VALUES OF DIPOLE MOMENT MATRIX ELEMENT USING SLATER TYPE ORBITALS

A. Dipole moment for ligand orbitals

The strength of the drive used in the orbital hybridization scheme depends on the value of the dipole moment operator between the two orbitals. Here, we have used Slater type orbitals [8] to calculate these dipole moments. The wavefunction of these orbitals is given by:

$$|\Psi_{n,l,m}(\mathbf{r})\rangle = R_n(r)Y_l^m(\mathbf{r}), \tag{26}$$

where

$$R_n(r) = (2\zeta)^n\sqrt{\frac{2\zeta}{(2n)!}}r^{n-1}e^{-\zeta r}, \tag{27}$$

with $\zeta = \frac{Z^*}{n}$ and Z^* is the effective charge which can be calculated using Slater's rules when distances are expressed in atomic units (1 unit $=a_0$). Using these Slater type orbitals, we approximate the expectation value of the position operator for different ligand and transition metal orbitals as shown in Table I.

B. Dipole moment for *d-d* transitions

In addition to the dipole transitions between different parity orbitals in the ligand ion, we also studied the effects of on-site *d-d* transitions. Although for pure *d* orbitals this kind of transitions are forbidden, but there are many different *d-p* mixing mechanisms available in transition metal compounds which allow these dipole transitions. In most of the transition metal compounds, e_g and t_{2g} orbitals are not purely of *d* character but has some contribution from *p* orbitals. These *p* orbitals can either belong to the same magnetic ion or to the ligand ion. In the absence of a center of symmetry, the t_{2g} orbitals can mix with *p* orbitals of the same ion. These *d* orbitals can also mix with the *p* orbitals of the ligand ion due to covalency efffects. This kind of mixing is allowed for both tetrahedral and octahedral crystal fields and is one of the most prominent mechanism for *d-p* mixing as indicated by the studies of the intensities of *d-d* observed in many transition metal compounds [9–12]. In transition metal compounds, the outermost electrons reside in *d* orbitals and the covalent bonding between the metal and the ligand ion can result in *d-p* mixing, and hence modifying the wavefunction of *d* orbitals as follows:

$$|\psi'_{d_i}\rangle = \frac{1}{\sqrt{1+\alpha^2}}\left(|\psi_{d_i}\rangle + \alpha\,|\chi_p\rangle\right), \tag{28}$$

where χ denotes the orbitals of ligand ions and $\alpha \ll 1$ (check Ref. [13] for more details of *d-p* mixing). As a result, the dipole moment operator $e\left|\left\langle\psi'_{t_{2g}}|\mathbf{r}|\psi_{e_g}\right\rangle\right| \approx e\left|\frac{\alpha}{\sqrt{1+\alpha^2}}\left\langle\psi_{3d_{z^2-r^2}}|\mathbf{r}|\chi_{p_z}\right\rangle\right|$ depends on the arrangement of ligand ions around the metal ion. This quantity can be estimated from Slater like orbitals if the mixing parameter is known which is usually difficult to determine. Since, this dipole moment is also proportional to the oscillator strength which can be calculated directly from the absorption spectra of these complexes. In some tetrahedral complex salts [11], the dipole moment between two different *d* orbitals belonging to t_{2g} and e_g sets can be as high as 0.5 Debye$= 0.1e\mathring{A}$. This kind of *d-d* transition also occur in some transition metal trichalcogenides like $NiPS_3$ [14] but the associated dipole moment would be much smaller as indicated by the extremely weak absorption for this peak.

Element	A	B	$\langle\psi_A\|\mathbf{r}\|\psi_B\rangle$
O	$2s$	$2p_z$	$0.6\,a_0\,\hat{z}$
S	$3s$	$3p_z$	$1.1\,a_0\,\hat{z}$
Sc	$3d_{z^2-r^2}$	$3p_z$	$0.3\,a_0\,\hat{z}$
Mn	$3d_{z^2-r^2}$	$4p_z$	$1.0\,a_0\,\hat{z}$

TABLE I: Position operator matrix elements between different orbitals calculated using Slater type orbitals.

V. VIBRONIC COUPLING ESTIMATE

In this section, we calculate the matrix element between two *d* orbitals for a phonon drive. We assume that the transition metal ion is surrounded by an octahedral arrangement of ligand ions, and the phonon mode involves the symmetric motion of ligand ions perpendicular to the metal ligand bond. For the geometry shown in Fig. 5, the potential around TM ion due to ligand ions is given by

$$V(\mathbf{r},t) = \sum_{L=1}^{8}\frac{q_L e^2}{4\pi\epsilon_0|\mathbf{a}_L(t)-\mathbf{r}|} \tag{29}$$

where q_L is the charge on ligand ion (in units of e), $\mathbf{a}_L$ is the position vector of ligand L from the center of the TM ion, and

$$\mathbf{a}_L(t) = \mathbf{a}_L^0 + \mathbf{u}_L(t) \tag{30}$$

where $\mathbf{a}_L^0$ is the equilibrium distance of M-L bond, and $\mathbf{u}_L$ is the phonon amplitude. For small $\mathbf{u}_L$, we can expand V around its equilibrium value as follows:

$$V(\mathbf{r},t) = \frac{q_L e^2}{4\pi\epsilon_0}\sum_{L=1}^{8}\left(\frac{1}{|\mathbf{a}_L^0-\mathbf{r}|} - \frac{(\mathbf{a}_L^0-\mathbf{r})\cdot\mathbf{u}_L(t)}{|\mathbf{a}_L^0-\mathbf{r}|^3} + ...\right), \tag{31}$$

and thus upto first-order, the perturbation is given by:

$$H' \approx -\frac{q_L e^2}{4\pi\epsilon_0}\sum_{j}^{8}\frac{(\mathbf{a}_L^0-\mathbf{r})\cdot\mathbf{u}_L(t)}{|(a_L^0)^2+r^2|^{\frac{3}{2}}}\left(1+3\frac{\mathbf{a}_L^0\cdot\mathbf{r}}{|(a_L^0)^2+r^2|} + ...\right). \tag{32}$$

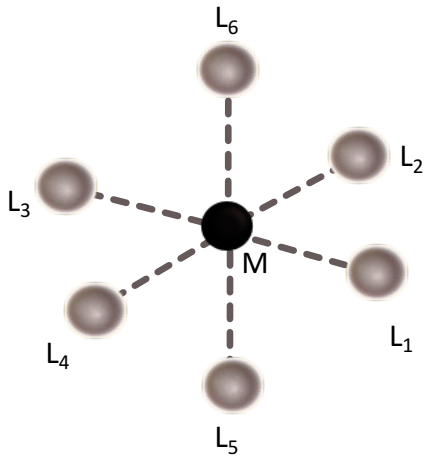

FIG. 5: Arrangement of ligand ions around a transition metal ion in octahedral geometry.

Now, the only terms which can couple two d orbitals are:

$$\langle d_\alpha|H'|d_\beta\rangle = \frac{3q_L e^2}{4\pi\epsilon_0}\sum_{L=1}^{8}\left\langle d_\alpha\left|\frac{(\mathbf{r}\cdot\mathbf{u}_L(t))(\mathbf{a}_L^0\cdot\mathbf{r})}{|(a_L^0)^2+r^2|^{\frac{5}{2}}}\right|d_\beta\right\rangle. \quad (33)$$

Furthermore, the matrix element $\langle d_\alpha|\mathbf{r}_k\mathbf{r}_l|d_\beta\rangle$ is non-zero for the cases shown in Table II.

d_α	d_β	$\mathbf{r}_k\mathbf{r}_l$	$\langle d_\alpha\|\mathbf{r}_k\mathbf{r}_l\|d_\beta\rangle$ $(\AA^2)$
d_{xy}	d_{yz}	xz	0.4
d_{xy}	d_{xz}	yz	0.4
d_{yz}	d_{xz}	xy	0.4
d_{yz}	$d_{x^2-y^2}$	yz	0.4
d_{xz}	$d_{x^2-y^2}$	xz	0.4
d_{xy}	$d_{z^2-r^2}$	xy	0.4
d_{yz}	$d_{z^2-r^2}$	yz	0.2
d_{xz}	$d_{z^2-r^2}$	xz	0.2

TABLE II: Matrix element $\langle\mathbf{r}_k\mathbf{r}_l\rangle$ between two $3d$ orbitals of Ti calculated using Slater type orbitals.

In $RTiO_3$, the ligand-metal distance, $|a_L^0| \approx 2\AA$, and thus the matrix element coupling two d orbitals becomes:

$$|\langle d_\alpha|H'|d_\beta\rangle| \approx 0.5u(t)\text{eV} = 0.25(e^{i\omega t}+e^{-i\omega t})u_0\text{eV} \quad (34)$$

for a g symmetry phonon mode, where u_0 is the displacement (in units of $\AA$) of the ligand ion perpendicular to the M-L bond.

VI. EXCITATION MECHANISM FOR THE RAMAN MODE COUPLED TO IR MODE

In Mott insulating titanates $YTiO_3$ and $LaTiO_3$ some of the Raman modes can be excited by making use of non-linear phonon coupling between different phonons.

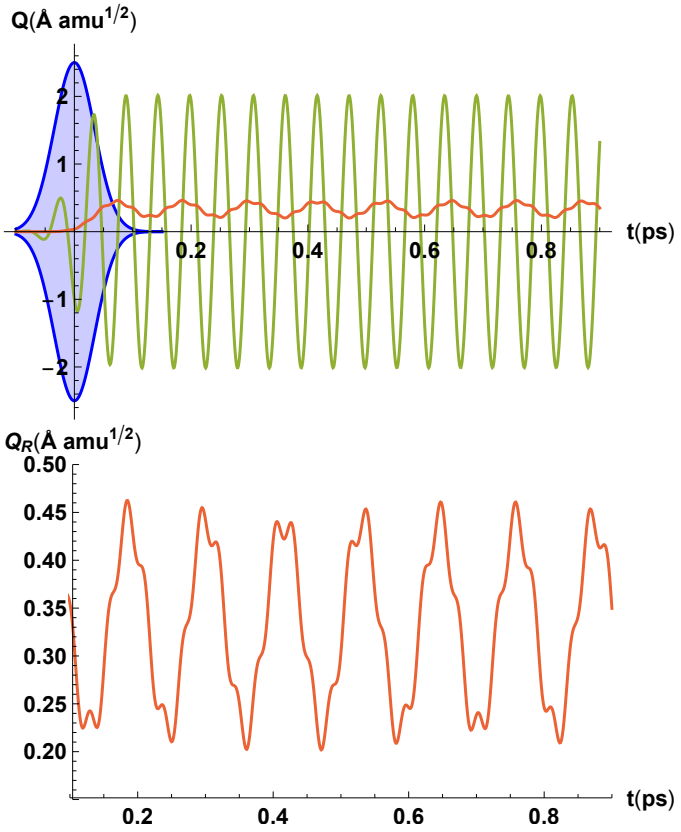

FIG. 6: Upper panel: Time evolution of Raman mode $A_g(25)$ (red curve) and IR active mode $B_{1u}(54)$(green) when excited by a resonant mid IR laser pulse of maximum amplitude $E = 0.5V/\AA$ and pulse width $\sigma = 50/\sqrt{2}fs$ (shown in blue envelope for illustration purpose). Lower Panel: Magnified version of Raman mode and the lattice vibrations are almost sinusoidal. Here the amplitude of $A_g(25)$ mode is $Q_R \approx 0.12\AA\sqrt{amu}$ and is proportional to the square of the amplitude of IR mode.

In the presence of an oscillating E field which excites the IR mode, the time-evolution of different phonon modes is governed by the following equations:

$$\ddot{Q}_{IR} = -\omega_{IR}^2 Q_{IR} + F(t) - 2gQ_R Q_{IR} - b_4 Q_{IR}^3 \quad (35)$$

$$\ddot{Q}_R = -\omega_R^2 Q_R - gQ_{IR}^2 - a_3 Q_R^2 \quad (36)$$

where $\omega_{R,IR}$ and $Q_{R,IR}$ are the frequencies and amplitudes of Raman and IR modes, respectively as discussed in Ref. [15]. Here the mode amplitude Q is measured in $\AA\sqrt{amu}$, ω_R^2 in units of $eV/(\AA\sqrt{amu})^2$ ($521.471cm^{-1} = 1eV/\AA^2 amu$), g in units of $eV/(\AA\sqrt{amu})^3$, and $F(t) =$

$CE\cos\omega t e^{-t^2/2\sigma^2}$ where E is measured in units of $V/\mathring{A}$ and $C = Z^*/\sqrt{m}$ depends on Born effective charge $Z^*$and $\sqrt{m}$ is the reduced mass of the mode. In the present scenario we can get the required rotation of oxygen octahedra by exciting $A_g(25)$ Raman mode. This mode couples strongly with IR mode $B_{1u}(54)$ with $g = 0.05$. Now, the amplitude of $A_g(25)$ Raman mode depends on a lot of factors like the coupling strength g, frequency ratio $\omega_{IR}/\omega R$, detuning $\omega - \omega_{IR}$, the pulse width σ. For the case of $YTiO_3$ and $LaTiO_3$, the time-evolution of above two equations for $E = 0.5V/\mathring{A}$ and $\sigma = 50/\sqrt{2}fs$ results in oscillations of amplitude $Q_R \approx 0.12\mathring{A}\sqrt{amu}$ which correspondents to a lattice oscillation of amplitude $u_0 \approx 0.02\mathring{A}$ as shown in Fig.6. We have ignored the damping terms as the damping would not affect the oscillations much for the time interval shown in the figure. Although the mode amplitude of IR active mode is large but since the other non-linear terms in Eq. 36 are usually small ($a_3 \approx 0.008eV/\mathring{A}^2/\sqrt{amu}^{3/2}$, $b_4 \approx 0.08eV/\mathring{A}^4/(amu)^2$) for similar orthorhombic structures [16] so these non-linear terms are irrelevant for the time-evolution in the regime considered here.

[1] J. Mentink, Journal of Physics: Condensed Matter **29**, 453001 (2017).
[2] J. H. Mentink and M. Eckstein, Phys. Rev. Lett. **113** (2014), 10.1103/PhysRevLett.113.057201, arXiv:1401.5308.
[3] J. Mentink, K. Balzer, and M. Eckstein, Nat. Commun. **6**, 6708 (2015).
[4] M. Bukov, M. Kolodrubetz, and A. Polkovnikov, Phys. Rev. Lett. **116**, 1 (2016), arXiv:1510.02744.
[5] J. Liu, K. Hejazi, and L. Balents, Phys. Rev. Lett. **121**, 107201 (2018).
[6] K. Hejazi, J. Liu, and L. Balents, arXiv:1809.09800 (2018).
[7] J. Liu, K. Hejazi, and L. Balents, arXiv:1801.00401.
[8] J. C. Slater, Phys. Rev. **36**, 57 (1930).
[9] C. Naiman, The Journal of Chemical Physics **35**, 323 (1961).
[10] A. D. Liehr and C. Ballhausen, Physical Review **106**, 1161 (1957).
[11] C. Ballhausen and A. D. Liehr, Journal of Molecular Spectroscopy **2**, 342 (1958).
[12] C. Ballhausen and A. D. Liehr, Molecular Physics **2**, 123 (1959).
[13] S. Sugano and R. G. Shulman, Phys. Rev. **130**, 517 (1963).
[14] S. Y. Kim, T. Y. Kim, L. J. Sandilands, S. Sinn, M.-C. Lee, J. Son, S. Lee, K.-Y. Choi, W. Kim, B.-G. Park, C. Jeon, H.-D. Kim, C.-H. Park, J.-G. Park, S. J. Moon, and T. W. Noh, Phys. Rev. Lett. **120**, 136402 (2018).
[15] M. Gu and J. M. Rondinelli, Phys. Rev. B **98**, 024102 (2018).
[16] A. Subedi, A. Cavalleri, and A. Georges, Phys. Rev. B **89**, 220301 (2014).